UNIVERSITY of
BRADFORD

Library

The University of Bradford Institutional Repository

http://bradscholars.brad.ac.uk

Link to publisher's version: *http://dx.doi.org/10.1039/C4CE00043A*

Citation: Seaton CC (2014) Proton location in acid···pyridine hydrogen bonds of multi-component crystals. CrystEngComm. 16(26): 5878-5886.

ARTICLE TYPE

Proton Location in Acid...Pyridine Hydrogen Bonds of Multi-Component Crystals.

Colin C. Seaton,[*a,b]

The design of new functional crystalline materials requires an understanding of the factors that control salt and co-crystal formation. These states often only differ in the location of the proton and are influenced by chemical and crystallographic factors. The interaction between a carboxylic acid and a pyridine is a frequently used supramolecular synthon in crystal engineering which can exist as either a co-

10 crystal ($CO_2H...N$) or salt ($CO_2^-...HN^+$). The results of a Cambridge Structure Database search indicate that the nature of the functional groups on the pyridine play a stronger role in selection of the phase than those of the acid. However, the nature of the local hydrogen bonding of the interaction also adjusts the potential for proton transfer. This was demonstrated by *ab initio* modelling of the energy landscape for binary and ternary co-crystals by inclusion of varying components of the local environment.

15 ## Introduction

The objectives of crystal engineering include the designed creation of novel materials through control of intermolecular interactions. Recently, multi-component crystals such as co-crystals and salts have become a key resource in achieving this

20 objective,[1,2] especially within the area of pharmaceutical materials.[3-5] They allow for the modification of physicochemical properties without altering the chemical structure of the components. The application of supramolecular synthons[6] is a key design tool in co-crystallisation to predict the potential

25 interactions between the selected components. However, many of the commonly utilised functional groups (e.g. carboxylic acids, N-heterocycles) are acidic or basic and so competition between the neutral co-crystal formation and the proton transfer salt can occur. This proton transfer process can also occur within the

30 solid-state in response to external factors, for example within carboxylic acid dimers with temperature[7] or between acidic and basic functional groups with pressure.[8] This can result in changes to the physicochemical properties such as colour or conductivity. Identification of whether a system exists as a salt or co-crystal

35 can also have regulatory significance, following the recent guidelines from the FDA on pharmaceutical co-crystals,[9] which indicate that a co-crystal system would be considered as a new drug formulation while salts would be considered as a new chemical species.

40 The level of proton transfer is controlled by both chemical and crystallographic factors. For example, the proton disorder in the acid dimer in 4-(dimethylamino)benzoic acid can be removed through co-crystallisation with 3,5-dinitrobenzoic acid and returned by creation of a ternary co-crystal with 3,5-

45 dintrobenzoic acid and 4,4'-bipyridine.[10-12] In this case while the chemical environment (same molecules interacting) is constant,

the local crystallographic environment changes with differences in the nature of the groups hydrogen bonding onto the dimer. Understanding how chemical and crystallographic factors

50 influence the final state of a system and if this can be controlled is an important contribution to the creation of novel functional materials.

The influence of chemical structure on proton location has, in general, been investigated by consideration of pK_a differences

55 between the two components.[13] This has lead to the development of the ΔpK_a rule, which indicates that salt formation is favoured for differences greater than three and co-crystals when the difference is less than zero. The region between these values displays mixed results with increased numbers of salts present for

60 larger differences.[14] While the ΔpK_a rule gives a good rule of thumb, there are limitations. The pK_a values are valid only for the solvent they were measured in (frequently water) and different systems vary to differing extents depending on the solvent. For example, 3,5-dinitrobenzoic acid has an aqueous pK_a of 3.45 and

65 a methanolic pK_a of 7.38, while pyridine has an aqueous pK_a of 5.22 and a methanolic pK_a of 5.44.[15] Computational methods for deriving pK_a values are calibrated to reflect the aqueous values but differing methods give rise to differing values and can display unrealistic trends.[16] Calculated values for 3,5-dinitrobenozic acid

70 include 3.3 (ChemAxon), 2.77 (ACD/Labs) and for pyridine 5.12 (ChemAxon) and 5.23 (ACD/Labs). Thus systems may be predicted to have different outcomes depending on the values chosen. Other methods of characterising the influence of chemical structure on the proton transfer may offer

75 complementary insights to the use of pK_a. Hammett substitution constants (σ)[17] are an empirical set of parameters generated for common functional groups, which are frequently used in physical organic chemistry to quantify electron withdrawing and donating capability of functional groups. They have been shown to

correlate with co-crystal formation for acid/acid systems[18-20] and benzamide/substituted benzoic acids.[21] Thus they may be applicable for the correlation of chemical factors on the proton transfer process and so a database study on substituted benzoic acids and pyridines has been undertaken to identify whether this is possible for these systems.

However, as both pK_a and Hammett constants are only molecular descriptors, the influence of the local crystal environment will not be reflected in any analysis based only on these values. Identifying the influence of local environment requires alternative methodologies. Creation of ternary multi-component systems (e.g. with three independent molecules) offer one such route as it may be possible to create a number of different environments for a given binary pair by variation of the third component. In the case of 3,5-dinitrobenzoic acid with 4,4'-bipyridine, a series of ternary complexes with 4-(dimethylamino)benzoic acid, 4-aminobenozic acid, 4-aminoslaicylic acid and sulfanilamide indicated that the position of the proton in the acid...pyridine dimer could be altered by the nature of the hydrogen bonding on the acid oxygen.[22]

Co-crystallisation of 3,5-dinitrobenzoic acid (**1**, Figure 1) with isonicotinamide (**a**, Figure 1) offers an ideal system to further investigate these ideas. A 1:1 salt (**1.a**) and a 1:2 co-crystal (**1.a.1**) have been reported.[23] Compound **1.a.1** features an elongated OH bond suggesting a possibly disordered hydrogen atom. Co-crystal formation is predicted for this system as ΔpK_a in water is 0.22 and in methanol it is –3.26.[§] Thus the crystal environment must play a role in adjusting the protonation state. A number of ternary co-crystals between **1** and **a** and substituted benzoic or cinnamic acids are also known.[24-26] In all cases the acid to pyridine interaction is of a co-crystal type and so the presence of the third acid must be the source of adjustment to the energy landscape. To develop a better understanding of this, crystals of the binary salt and a new ternary complex with 3-aminobenzoic acid (**1.a.2**, Figure 1) were grown and the energetics of the proton transfer determined by *ab initio* calculations on small molecule clusters. The crystal structure of a second system between 2,4,6-trihydroxybenzoic acid (**3**, Figure 1) and isonicotinamide (**3.a**) was also determined and studied by these computational methods to confirm their applicability to other systems.
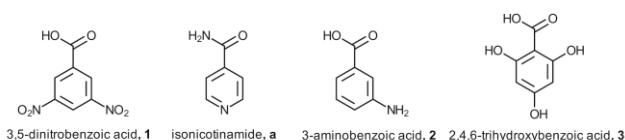

Figure 1. Chemical structures of the compounds studied

Experimental Methodology

All chemicals were purchased from Sigma-Aldrich and used as received.

Crystallisation of 3,5-dinitrobenzoic acid/isonicotinamide (1.a)

3,5-Dinitrobenzoic acid (0.11 g, 0.1 mmol) and isonicotinamide (0.06 g, 0.5 mmol) were dissolved in methanol (5 cm^3) with gentle heating. Upon removal from the hot plate the sample was left to cool. Clear plate-like crystals of **1.a** grew upon standing with slow evaporation of the solvent.

Crystallisation of 2,4,6-trihydroxybenzoic acid/isonicotinamide (3.a)

2,4,6-Trihydroxybenzoic acid monohydrate (0.12 g, 0.7 mmol) and isonicotinamide (0.06 g, 0.5 mmol), were dissolved in methanol (7.5 cm^3). The sample was heated to ensure complete dissolution, removed from the hot plate and left to cool to room temperature. Upon slow evaporation, light brown blocky crystals of **3.a** were produced.

Crystallisation of 3,5-dinitrobenzoic acid/isonicotinamide/3-aminobenzoic acid (1.a.2)

3,5-Dinitrobenzoic acid (0.09 g, 0.4 mmol), 3-aminobenzoic acid (0.06 g, 0.4 mmol) and isonicotinamide (0.05 g, 0.4 mmol) were dissolved in methanol (5 cm^3) with gentle heating. The sample was removed from the hot plate and after cooling the solution was left to slowly evaporate. After a few days colourless plate-like crystals were formed, which were identified by single crystal X-ray diffraction as samples of **1.a**. On standing for a further week, crystallisation of yellow blocky crystals of **1.a.3** occurred with the simultaneous dissolution of the colourless crystals of **1.a**.

Crystal Structure Determination

Crystal structures for **1.a**, **3.a** and **1.a.2** (Figures S1, S2, S3 in the ESI) were determined using an Agilent Xcalibur single crystal diffractometer with monochromated Mo Kα radiation at 100 K (Table 1).[‡] The structures of **1.a** and **1.a.2** were solved by direct methods in the program SHELXS,[27] while the structure of **3.a** was determined by direct methods in the program SIR92.[28] All structures were subsequently refined using SHELXL2013[27] in the program OLEX2.[29] Hydrogen atoms were treated by a mixture of independent and constrained refinement with the hydrogen atoms bonded to oxygen or nitrogen atoms located in the difference maps and then freely refined while hydrogen atoms bonded to carbon atoms were treated as riding.

Computational Methodology

The selected dimers, trimers and tetramers were extracted from the relevant crystal structures such that the molecular orientation for each molecule was the same in all cases. Initially the clusters were optimised by DFT calculations using the program ORCA (PBE-D3/def2-TZVP).[30-33] In the case of **1/a** systems only the hydrogen atom locations were optimised, while a full optimisation was performed in the case of **3/a**. The proton transfer energy surfaces of the **1/a** systems were constructed by positioning the acid hydrogen at different fixed distances from the acid oxygen and evaluated by DFT calculations (PBE-D3/def2-TZVPP) in the ORCA program. For the **3/a** systems, the energy of an fully optimised system at each O–H distance was evaluated. To simulate the polarising environment of the crystal structure the calculations were performed using the COSMO methodology[34] with a dielectric constant of three.

Table 1. Crystal Data and Structure Refinement for **1.a**, **3.a** and **1.a.2**

System	**1.a**	**3.a**	**1.a.2**
Empirical formula	C13 H10 N4 O7	C13 H12 N2 O6	C20 H17 N5 O9
Temperature (K)	100(2)	100(2)	100(2)
Wavelength (Å)	0.71073	0.71073	0.71073
Crystal system	Triclinic	Orthorhombic	Triclinic
Space group	P -1	Pna2$_1$	P -1
a, b, c (Å)	7.2376(6), 8.9810(8), 10.8011(8)	12.8093(14), 13.1563(12), 7.4708(8)	7.0678(4), 8.8189(5), 16.2172(9)
α, β, γ (°)	87.807(7), 76.086(7), 87.040(7)	90, 90, 90	93.761(5), 90.458(5), 95.498(5)
Volume (Å^3)	680.33(10)	1259.0(2)	1003.90(10)
Z, density (Mg/m^{-3})	2, 1.632	4, 1.542	2, 1.559
Crystal size (mm^3)	0.9 × 0.6 × 0.32	0.6 x 0.4 x 0.3	0.5 × 0.2 × 0.1
Theta range for data collection (°)	3.029 to 28.420.	3.136 to 28.419	3.141 to 28.253
Index ranges	-9 ≤ h ≤ 9 -12 ≤ k ≤ 7 -13 ≤ l ≤ 12	-16 ≤ h ≤ 9 -17 ≤ k ≤ 15 -9 ≤ l ≤ 3	-9 ≤ h ≤ 9 -11 ≤ k ≤ 6 -20 ≤ l ≤ 21
Reflections collected/independent [R(int)]	4505 / 2998 [0.0299]	3389 / 1815 [0.0597]	7010 / 4447 [0.0296]
Data / restraints / parameters	2998 / 0 / 257	1815 / 1 / 238	4447 / 0 / 331
Goodness-of-fit on F^2	0.974	0.825	0.781
Final R indices [I>2σ (I)]	R1 = 0.0430, wR2 = 0.1102	R1 = 0.0352, wR2 = 0.0453	R1 = 0.0376, wR2 = 0.0585
R indices (all data)	R1 = 0.0603, wR2 = 0.1181	R1 = 0.0588, wR2 = 0.0482	R1 = 0.0843, wR2 = 0.0634
Largest diff. peak and hole (e.Å^{-3})	0.356 and -0.332	0.180 and -0.227	0.244 and -0.220

Database Analysis

CSD version 5.34 with 2 updates was searched using Conquest (V1.15)[35,36] for structures containing a benzoic acid and pyridine with a short contact between the carboxylic/carboxylate group and the pyridine/pyridinium. The search was limited to organic compounds with functional groups that had published Hammett constants (*m*- and *p*- substituted only). The structures were then categorised into co-crystal (OH...N interaction), salt (O$^-$...HN$^+$ interaction) and disordered systems (O...H...N). As the majority of structures available are determined by X-ray diffraction, the location of the hydrogen atom of interest can be misleading due to the weak diffraction of the hydrogen or it has been placed in a calculated position. For example, the system between 3,5-dinitrobenzoic acid and nicotinic acid was initially determined by X-ray diffraction as a co-crystal system (AWUDEB), however a subsequent neutron diffraction studies shows salt formation (ZIKQOB).[37] Thus consideration of the C–O distances in the carbonyl group was also used when assigning structures to specific classifications. Systems that displayed variation in hydrogen location with temperature were assigned to the disordered systems category. pK$_a$ values for each system were calculated using ChemAxon accessed through the Chemspider webpage, while Hammett constants were taken from Hansch *et al.*.[17]

Results and Discussion

Crystal Structure Analysis

Compound **1.a** is a 1:1 salt with a $^+$NH...O$^-$ hydrogen bond (Table 2) linking the components into a dimer. The C-O distances of **1**

are in the range of values expected for a carboxylate ion (d$_{c-o}$ = 1.239(2)/1.261(2) Å). Pairs of dimers form a tetramer through an R$_2^2$(8) amide...amide hydrogen bond. This tetramer packs into a 1-D ribbon along the *b*-axis through N–H...O$_{carbonyl}$ hydrogen bonds. These ribbons are linked by weaker C–H...O$_{nitro}$ hydrogen bonds (R$_2^2$(10) motif) forming a 2-D sheet (Figure 2). The final structure is formed by packing of these sheets through C–H...O$_{nitro}$ hydrogen bond between the ring hydrogen of **a** and a nitro group of **1** forming a R$_2^2$(7) motif.

### Table 2. Hydrogen bonding in **1.a** crystal structure.

D-H...A	d$_{DH}$/Å	d$_{H...A}$/Å	d$_{D...A}$/Å	D-H...A
N2B–H2BA...O1B (−x, −y−1, −z)	0.92(2)	2.01(2)	2.9272(19)	177.2(18)
N2B–H2BB...O2A (x, y-1, z)	0.90(2)	1.99(2)	2.8759(19)	166.3(19)
N1B–H1B...O1A (x, y, z)	0.99(2)	1.57(2)	2.5370(18)	163(2)
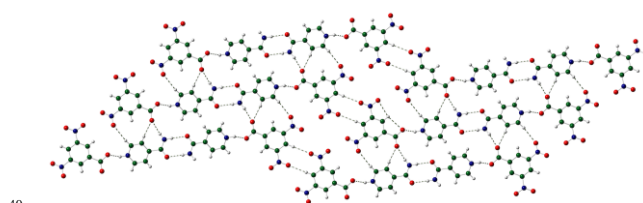
Figure 2. Formation of 2-D in **1.a** through combination of strong and weak hydrogen bonds.

Compound **3.a** forms as a 1:1 salt with a $^+$NH...O$^-$ hydrogen bond (Table 3) linking the components into a dimer, however unlike **1.a**, the dimers are linked into a 1-D chain through OH...O$_{carbonyl}$ hydrogen bonds from the *para*-hydroxyl group of **3** and the amide O of **a** (Figure 3). Donation of the hydrogen atoms of the amide group on **a** to carboxylate and hydroxyl oxygens of **3** crosslink these chains forming the final 3-D crystal structure.

Table 3. Hydrogen bonding in **3.a** crystal structure

D-H...A	d$_{DH}$/Å	d$_{H...A}$/Å	d$_{D...A}$/Å	D-H...A
O28–H28···O31	0.85(3)	1.70(3)	2.491(3)	152(3)
O25–H25···O0AA	1.04(3)	1.55(3)	2.545(3)	158(3)
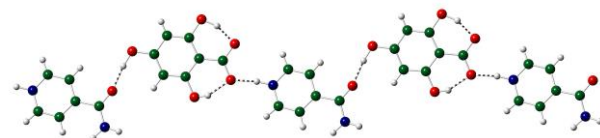
Figure 3. Formation of 1-D chain in **3.a**, through $^+$N–H...O$^-$ and O–H...O hydrogen bonds.

Compound **1.a.2** is a ternary co-crystal (1:1:1) and is isostructural with four of the other known ternary systems (CSD REFCODES: AJAKIF,[26] BUDZUV,[24] BUFBIP,[24] XAQPOV).[25] The OH bond length is elongated compared to other ternary complexes (Table 4), but as all structures have been determined from X-ray data and are at different temperatures, direct comparison may be misleading. However, in all cases, the system has greater co-crystal behaviour than salt as the hydrogen atom is

bonded to the carboxylic acid rather than the pyridine. Additionally the C-O distances in the **1** component are in the range expected for a carboxylic acid rather than a carboxylate (Table 5). The components are linked through an OH...N$_{pyridine}$ hydrogen bond between **1** and **a**, while a R$_2^2$(8) acid...amide dimer links **a** with **2**. These trimers are linked through a pair of NH...O hydrogen bonds (between the amide N of **a** to carbonyl O of **1** and the amino N of **2** to the carbonyl O of **a**) forming a 1-D ribbon motif along the *b*-axis. A 2-D sheet is formed from these ribbons through N–H...O$_{nitro}$ hydrogen bonds (Figure 4) and the final 3-D structure is completed through packing of these sheet by weaker C–H...O and π...π interactions.

Table 4. Hydrogen bonding in **1.a.2** crystal structure.

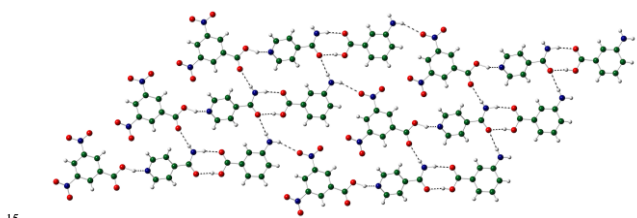| D-H...A	d_{DH}/Å	$d_{H...A}$/Å	$d_{D...A}$/Å	D-H...A
N2B–H2BA⋯O2C (x, y+1, z)	0.967(19)	1.96(2)	2.9115(19)	168.6(15)
O1C–H1C⋯O1B (x, y-1, z)	0.99(2)	1.62(2)	2.5946(16)	165.8(19)
N1C–H1CA⋯O1C (x, y+1, z)	0.91(2)	2.63(2)	3.118(2)	113.9(15)
N1C–H1CA⋯O1B (x+1, y+1, z+1)	0.91(2)	2.14(2)	3.049(2)	172.2(17)
N1C–H1CB⋯O4A	0.93(2)	2.49(2)	3.333(2)	150.2(17)
N2B–H2BB⋯O2A (x, y+1, z)	0.864(18)	2.059(19)	2.9123(19)	169.6(18)
O1A–H1A⋯N1B	1.10(2)	1.55(2)	2.6093(17)	161.6(18)

Figure 4. Formation of 2-D sheet in **1.a.2** through a combination of strong and weak hydrogen bonding.

Table 5. O-H distances in **1/a** ternary crystals

REFCODE	Third Component	Determination Temperature (K)	d_{OH}/Å	d_{C-O}/Å
AJAKIF	*p*-toluic acid (**1.a.4**)	173	0.90	1.205/1.288
BUDZUV	*m*-toluic acid (**1.a.5**)	203	0.94	1.214/1.294
BUFBIP	4-(dimethylamino)benzoic acid (**1.a.6**)	203	1.08	1.214/1.292
BUFQAU	4-hydroxy-3-methoxycinnamic acid (**1.a.7**)	203	1.20	1.217/1.301
XAQPOV	3,4-dimethoxycinnamic acid (**1.a.8**)	203	1.01	1.212/1.297
This Work	3-aminobenzoic acid (**1.a.2**)	100	1.10	1.218/1.309

Influence of local environment on proton location

For all three systems, the direct bonding environment around the acid/pyridine interaction is the same, with an amide nitrogen of **a**

hydrogen bonding to the carbonyl/carboxylate group of **1**. However, the bonding of the amide group is different in each case. In **1.a**, it forms an amide/amide dimer, while an acid/amide dimer is present in **1.a.2**. In contrast in **3.a** the amide group bridges across stacked pairs of dimers (Figure 5). This variation in the bonding environment of the components is expected to strongly influence the final proton location. This was investigated through *ab initio* calculations to construct energy landscapes for the various systems.
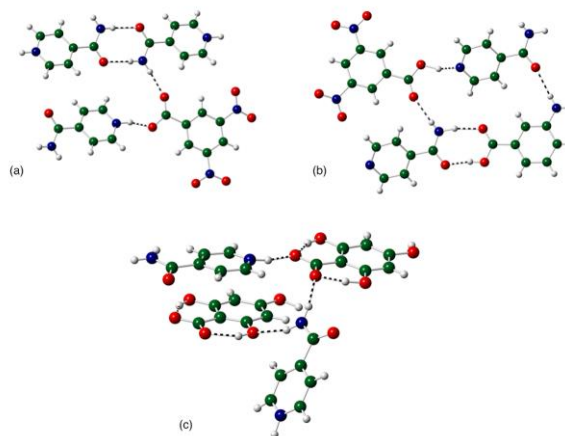

Figure 5. The local bonding environment of (a) **1.a**, (b) **1.a.2** and (c) **3.a**.

The energy landscape for proton transfer between **1** and **a** was constructed from DFT calculations of molecular clusters with increasing numbers of molecules (Figure 6). The OH distance was incrementally increased from 0.75 to 1.55 Å in steps of 0.1 Å, while the rest of the cluster was constrained to the crystal geometry. The initial gas phase optimisation of the isolated dimer resulted in the location of the co-crystal phase and a calculated surface displays a defined minimum around the co-crystal OH distance (~1.05 Å, Figure 7). It is well known that molecular geometry and properties can differ between gas phase calculations and the condensed phase. For example, gas phase optimisations may give different conformations compared to the crystal structure due to the lack of consideration of polarization by the crystal lattice.[38-41] It has been shown that improved conformations of polymorph prediction may be obtained using the Polarizable Continuum Model (PCM) to surround the system in a dielectric constant of three to approximate the crystal environment.[42,43] The application of such methodologies to the proton transfer calculations may also capture an approximation of the crystal influence on the proton transfer process and so the proton surface scan was repeated using the COSMO PCM methodology to create the dielectric box. This resulted in a broadening of the surface but the co-crystal form was still the lowest energy state (Figure 7).
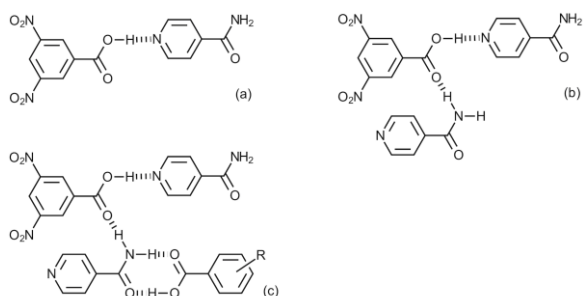
Figure 6. Schematic representations of the (a) dimer, (b) trimer and (c) tetramer structures constructed to model the **1/a** systems.
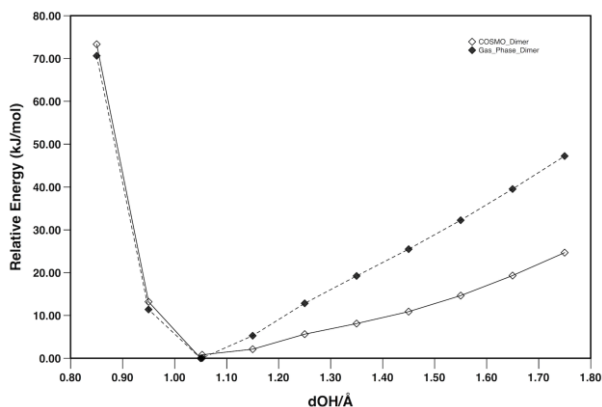

Figure 7. Plot of the relative energy of proton transfer between **1** and **a** in a dimer in both the gas phase (black diamonds) and in a COSMO box (ε = 3, white diamonds). Lines added for clarity.

Expanding the clusters to include a third component was initially done by adding a molecule of **a** (in both protonated and deprotonated forms (Figure 8)). The resulting surfaces show a shift in the position of the minimum of the surface, with a significant flattening (Figure 9). The presence of the protonated **a** favours a salt form (minimum energy at d_{OH} = 1.31 Å), while the deprotonated **a** causes an elongation of the OH co-crystal bond (minimum energy at d_{OH} = 1.16 Å). Thus introduction of the hydrogen bonding group alters the proton location in a way that reflects the experimental results. In the case of **1.a** the salt is formed by the bonding of the isonicotinamide molecule, while **1.a.1** has only weak C–H...O bonds and so favours the co-crystal phase.

Introduction of the third acid in the ternary systems results in a further alternation of the proton surface with a greater rise in the energy of the salt system (Figure 10). Generally, variation of the third component (from **2** to **4, 5, 6**) has little change on the observed surface suggesting that only the presence of the acid group is required to induce the structural change. However, the shape of the surface for **1.a.4** differs from the other systems, possibly due to the different atom location of the non-hydrogen atoms from each structure. Full optimisation of the clusters may be required to confirm this factor, however the resulting structure would differ from the situation present in the crystal structure. Further work is required both computationally and experimentally to investigate what range of third components can be introduced into this system and the influence of these changes on the crystal environment and protonation state of the components.
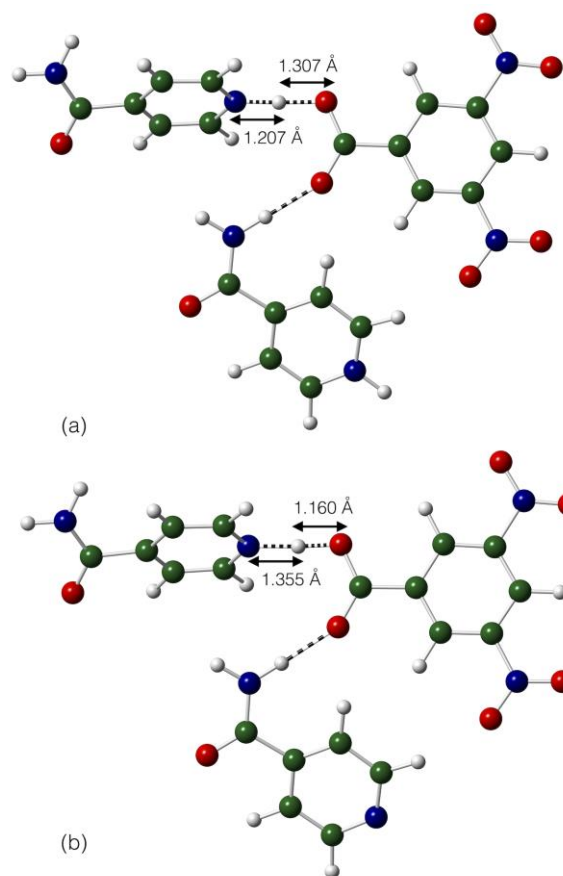

Figure 8. Comparison of the lowest energy structures of the trimers formed between **1, a** with (a) protonated **a** and (b) deprotonated **a**. N–H and O–H distances in the acid…pyridine interactions are indicated for each system.

Similar results are observed in the calculations for the **3/a** system (Figure 11) where a dimer and trimer system were modelled (Figure 12). The dimer system has a co-crystal minimum, while the trimer system has a salt minimum. In this system a complete optimisation of the structure was undertaken and while the geometry of the dimer is consistent with the crystal structure, the location of the third component of the trimer differs slightly from the crystal. However, given that the presence of the hydrogen bonding group appears to play a greater role than the geometry or nature of the system, the results are applicable for the consideration of the nature of the transfer. It appears suitable *ab initio* models of molecular clusters can offer a qualitative insight into the proton location. However, it requires knowledge of the type and geometry of the local hydrogen bonding present within the system. The development of fully predictive methods based on these calculations must be combined with an understanding of the reproducibility of the local hydrogen bonding environment for a desired hydrogen bond.
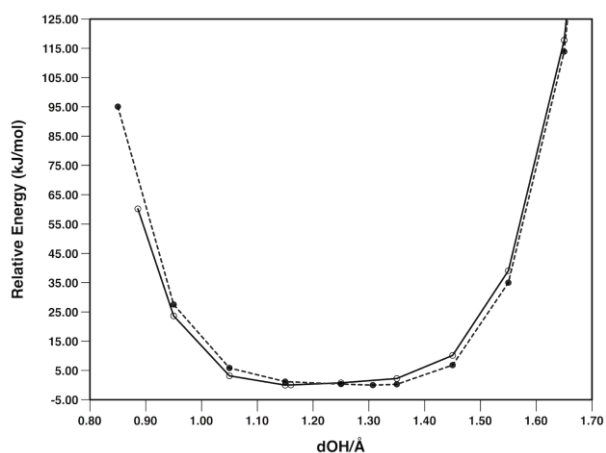
Figure 9. Plot of the relative energy of proton transfer between **1** and **a** in a trimer with a second **a** molecule (protonated: black circles, deprotonated: white circles) in a COSMO box (ε = 3). Lines added for clarity.
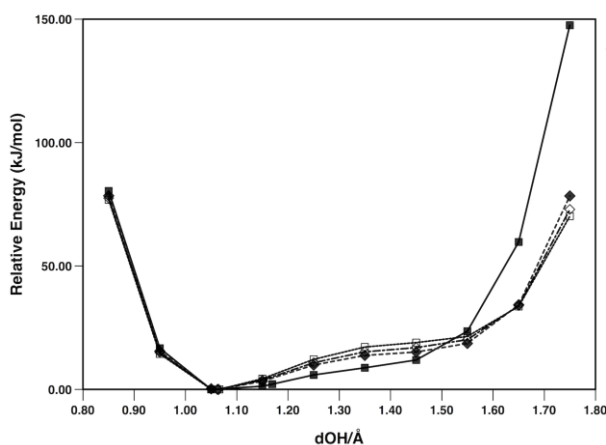

Figure 10. Plot of the relative energy of proton transfer between **1** and **a** in a tetramer with a second **a** and **2** (white squares), **4** (black squares), **5** (white diamonds) and **6** (black diamonds) in a COSMO box (ε = 3). Lines added for clarity.
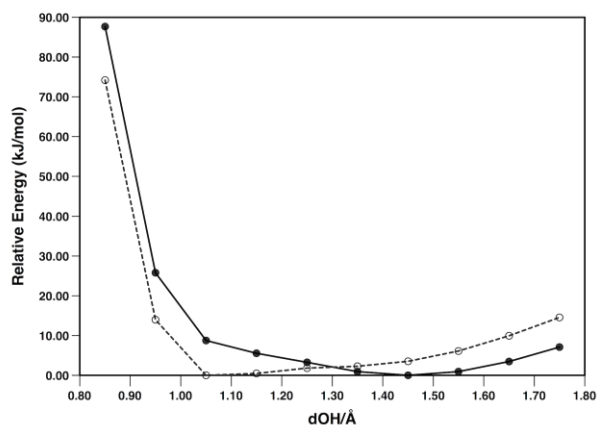

Figure 11. Plot of the relative energy of proton transfer between **3** and **a** in a dimer (white circles) and a trimer (black circles) in a COSMO box (ε = 3). Lines added as a guide for the eye.
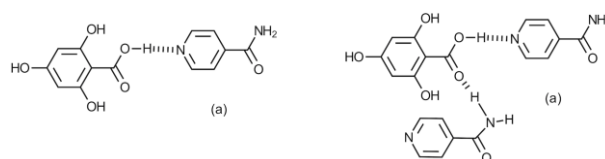

Figure 12. Schematic representations of the (a) dimer and (b) trimer structures constructed to model the **3**/**a** systems.

Database Analysis Results

Over a hundred structures with carboxylic acid and pyridine functional groups hydrogen bonded to each other were identified from the database search of which 59% were co-crystals, 34 % salts and the remaining 7 % disordered systems. Searches for other acidic and basic groups such as phosphoric acids, piperidines etc., either failed to locate enough structures for analysis or were all one type of structure (next largest group consisting of carboxylic acids with piperidine which had only 12 salts). The system follows the ΔpK_a rule with those systems with $\Delta pK_a > 3$ forming salts and those < 0 forming co-crystals (Figure 13). However, a range of outcomes is obtained in the intermediate region with few trends observed. However, calculated pK_a values have been used in this analysis and so errors in the values may mask some trends, along with the subjective nature of the clustering. The variation in product with Hammett constant (Figure 14) displays similar results to the pK_a plot, however, it suggests that the nature of the functional group on the pyridine molecule has a greater influence than the acid. This is shown by the general segregation of results around σ(base) = 0, where σ(base) is the Hammett constant of the functional group on the pyridine. Electron withdrawing groups (+σ, weaker bases) have a greater tendency to co-crystallisation, while electron donating groups (−σ, stronger bases) favour salt formation. The opposite trend would be expected for the acid groups (stronger acids with electron withdrawing groups, weaker acids with electron donating groups); while there is a slight increase in salts as σ(acid) (Hammett constant of the functional group on the benzoic acid) increases, there is a lack of clustering along the acid axis.
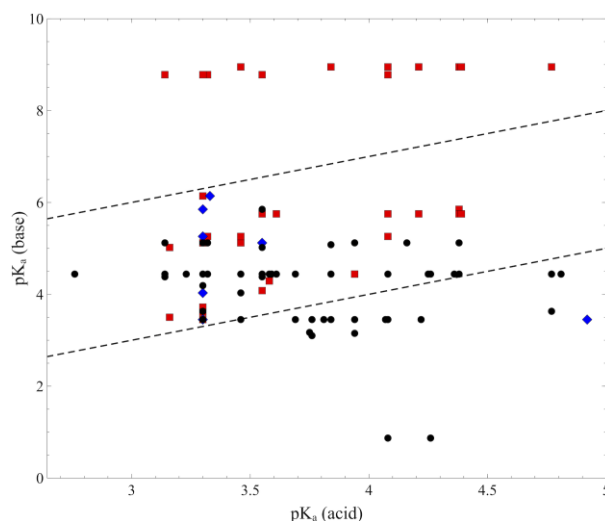

Figure 13. Plot of the pK_a of the base against the pK_a of the acid in the located crystal structures. Systems forming co-crystals are displayed as black circles, salt formers as red squares and disordered as blue diamonds. The two dotted lines correspond to $\Delta pK_a = 0$ and $\Delta pK_a = 3$.
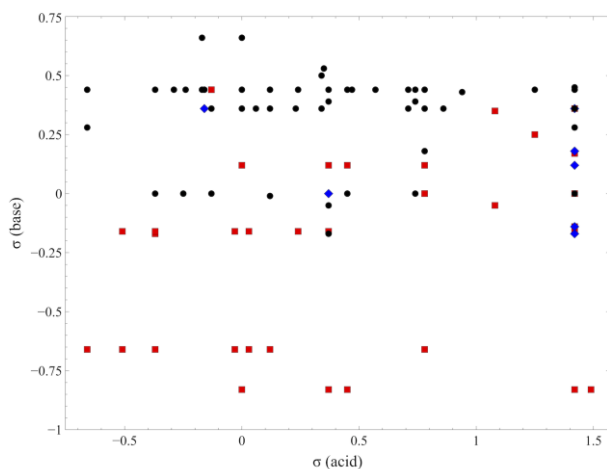
Figure 14. Plot of the Hammett constant of the base against the Hammett constant of the acid in the located crystal structures. Systems forming co-crystals are displayed as black circles, salt formers as red squares and disordered as blue diamonds.

As the Hammett constants are related to pK_a values (originial derivation of σ values was from the aqueous ionisation constant ($\sigma = \log K_X - \log K_H$[17] where K_H is the ionisation constant for benzoic acid in water at 25 °C, while K_X is constant for *meta-* or *para-* substituted benzoic acid), and a roughly linear trend is observed for the systems studied here, (ESI Figures S4, S5) a correlation between the two plots is expected. Removal of the systems where the ΔpK_a rule is successful indicates a partial segregation of the co-crystal forming systems (Figure 15). Thus a combination of ΔpK_a and Hammett constant may give an indication of outcome. However as some of the systems considered consist of the same species within different crystals structures (either polymorphs or different compositions) with different assignments, it must be noted that the crystal structure contributes to the outcome. The lack of consideration of any crystal structure influence is also the probable cause of the failure to fully segregate the systems since this factor is not considered by either of these measures. This will be a limitation of any method that considers only molecular structure in the prediction. However, the use of computational modelling to support such empirical analysis may increase the predictive ability within this area.
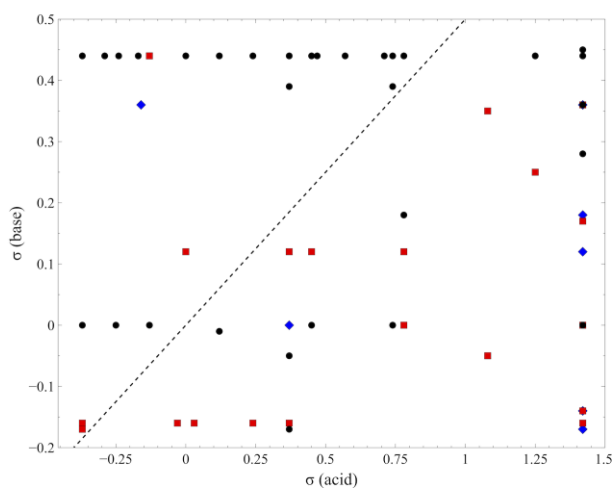

Figure 15. Re-plot of Figure 2 with systems successfully predicted by ΔpK_a rule removed. Dotted line [σ(base) = 0.5σ(acid)] indicates a partial segregation of the types.

Conclusions

Both chemical and crystallographic factors influence the underlying energy surfaces that result in a given system forming co-crystals or salts. While pK_a values and Hammett constants can be used to predict many of the chemical factors relating to these outcomes, the influence of local packing is a harder concept to quantify. For carboxylic acids and pyridines, the nature of the functional group on the pyridine appears to influence the outcome to a greater extent than the acid, with the majority of co-crystals forming from systems with functional group described by positive Hammett constants. Salts in contrast are more prevalent for pyridine systems that have functional groups with negative Hammett constants. However the presence of systems with the same intermolecular interaction in different crystal structures displaying different proton locations clearly indicates that crystal environment can play a decisive role. The use of computational methods to probe the energy surfaces relating to the proton transfer process can give a qualitative understanding of the role of chemical and crystallographic influences. The work suggests that developing methods for the design and creation of such proton transfer systems would require a greater understanding of the factors that influence the construction of the crystal environment beyond the pairwise association of the two components.

Notes and references

[a] Division of Chemistry and Forensic Science, School of Life Sciences, University of Bradford, Richmond Road, Bradford, UK, BD7 1DP. E-mail: c.seaton@bradford.ac.uk, Tel: +44(0)1274 236185.
[b] Synthesis and Solid State Pharmaceutical Centre, Materials and Surface Science Institute, University of Limerick, Ireland.

1. D. Braga, S. d'Agostino, E. Dichiarante, L. Maini, and F. Grepioni, *Chem. - Asian J.*, 2011, **6**, 2214–2223.
2. G. R. Desiraju, *Angew. Chem. Int. Ed.*, 2007, **46**, 8342–8356.
3. R. Thakuria, A. Delori, W. Jones, M. P. Lipert, L. Roy, and N. Rodriguez-Hornedo, *Int. J. Pharm.*, 2013, **453**, 101–125.
4. T. Friščić and W. Jones, *J. Pharm. Pharmacol.*, 2010, **62**, 1547–1559.
5. N. Shan and M. J. Zaworotko, *Drug Discov. Today*, 2008, **13**, 440–446.
6. G. R. Desiraju, *Angew. Chem. Int. Ed.*, 1995, **34**, 2311–2327.
7. C. C. Wilson, *Crystallogr. Rev.*, 2007, **13**, 143–198.
8. D. M. S. Martins, D. S. Middlemiss, C. R. Pulham, C. C. Wilson, M. T. Weller, P. F. Henry, N. Shankland, K. Shankland, W. G. Marshall, R. M. Ibberson, K. S. Knight, S. Moggach, M. Brunelli, and C. A. Morrison, *J. Am. Chem. Soc.*, 2009, **131**, 3884–3893.
9. Food and Drug Administration, *Guidance for Industry: Regulatory Classification of Pharmaceutical Co-Crystals*, Silver Spring, MD, USA, 2013.

10. A. Parkin, C. C. Seaton, N. Blagden, and C. C. Wilson, *Cryst. Growth Des.*, 2007, **7**, 531–534.

11. L. H. Thomas, N. Blagden, M. J. Gutmann, A. A. Kallay, A. Parkin, C. C. Seaton, and C. C. Wilson, *Cryst. Growth Des.*, 2010, **10**, 2770–2774.

12. A. O. F. Jones, N. Blagden, G. J. McIntyre, A. Parkin, C. C. Seaton, L. H. Thomas, and C. C. Wilson, *Cryst. Growth Des.*, 2013, **13**, 497–509.

13. S. L. Childs, G. P. Stahly, and A. Park, *Mol. Pharmaceutics*, 2007, **4**, 323–338.

14. A. J. Cruz Cabeza, *CrystEngComm*, 2012, **14**, 6362–6365.

15. F. Rived, M. Roses, and E. Bosch, *Anal. Chim. Acta*, 1998, **374**, 309–324.

16. T. Friščić, D. G. Reid, G. M. Day, M. J. Duer, and W. Jones, *Cryst. Growth Des.*, 2011, **11**, 972–981.

17. C. Hansch, A. Leo, and R. W. Taft, *Chem. Rev.*, 1991, **91**, 165–195.

18. C. C. Seaton, *CrystEngComm*, 2011, **13**, 6583–6595.

19. C. C. Seaton, K. Chadwick, G. Sadiq, K. Guo, and R. J. Davey, *Cryst. Growth Des.*, 2010, **10**, 726–733.

20. K. Chadwick, G. Sadiq, R. J. Davey, C. C. Seaton, R. G. Pritchard, and A. Parkin, *Cryst. Growth Des.*, 2009, **9**, 1278–1279.

21. C. C. Seaton and A. Parkin, *Cryst. Growth Des.*, 2011, **11**, 1502–1511.

22. C. C. Seaton, N. Blagden, T. Munshi, and I. J. Scowen, *Chem. - Eur. J.*, 2013, **19**, 10663–10671.

23. S. Tothadi and G. R. Desiraju, *Phil. Trans. R. Soc. A*, 2012, **370**, 2900–2915.

24. C. B. Aakeröy, A. M. Beatty, and B. A. Helfrich, *Angew. Chem. Int. Ed.*, 2001, **40**, 3240–3242.

25. C. B. Aakeröy, J. Desper, E. Elisabeth, B. A. Helfrich, B. Levin, and J. F. Urbina, *Z. Kristallogr.*, 2005, **220**, 325–332.

26. C. B. Aakeröy, A. M. Beatty, B. A. Helfrich, and M. Nieuwenhuyzen, *Cryst. Growth Des.*, 2003, **3**, 159–165.

27. G. M. Sheldrick, *Acta Crystallogr., Sect. A: Found. Crystallogr.*, 2008, **64**, 112–122.

28. A. Altomare, G. Cascarano, C. Giacovazzo, A. Guagliardi, M. C. Burla, G. Polidori, and M. Camalli, *J. Appl. Cryst.*, 1994, **27**, 435.

29. O. V. Dolomanov, L. J. Bourhis, R. J. Gildea, J. A. K. Howard, and H. Puschmann, *J. Appl. Cryst.*, 2009, **42**, 339–341.

30. F. Neese, *WIREs Comput. Mol. Sci.*, 2012, **2**, 73–78.

31. A. Schaefer, H. Horn, and R. Ahlrichs, *J. Chem. Phys.*, 1992, **97**, 2571.

32. F. Weigend and R. Ahlrichs, *Phys. Chem. Chem. Phys.*, 2005, **7**, 3297.

33. S. Grimme, J. Antony, S. Ehrlich, and H. Krieg, *J. Chem. Phys.*, 2010, **132**, 154104.

34. A. Klamt, *J. Phys. Chem.*, 1995, **99**, 2224–2235.

35. F. H. Allen, *Acta Crystallogr., Sect. B: Struct. Sci.*, 2002, **58**, 380–388.

36. I. J. Bruno, J. C. Cole, P. R. Edgington, M. Kessler, C. F. Macrae, P. McCabe, J. Pearson, and R. Taylor, *Acta Crystallogr., Sect. B: Struct. Sci.*, 2002, **58**, 389–397.

37. S. J. Ford, G. J. McIntyre, M. R. Johnson, and I. R. Evans, *CrystEngComm*, 2013, **15**, 7576–7582.

38. H. Nowell and S. L. Price, *Acta Crystallogr., Sect. B: Struct. Sci.*, 2005, **61**, 558–568.

39. S. L. Price, *Acta Crystallogr., Sect. B: Struct. Sci.*, 2013, **69**, 313–328.

40. J. Kendrick, G. A. Stephenson, M. A. Neumann, and F. J. J. Leusen, *Cryst. Growth Des.*, 2013, **13**, 581–589.

41. G. M. Day, W. D. S. Motherwell, and W. Jones, *Phys. Chem. Chem. Phys.*, 2007, **9**, 1693–1704.

42. T. G. Cooper, K. E. Hejczyk, W. Jones, and G. M. Day, *J. Chem. Theory Comput.*, 2008, **4**, 1795–1805.

43. A. V. Kazantsev, P. G. Karamertzanis, C. S. Adjiman, C. C. Pantelides, S. L. Price, P. T. A. Galek, G. M. Day, and A. J. Cruz Cabeza, *Int. J. Pharm.*, 2011, **418**, 168–178.

44. T. Dorn, K. Fromm, and C. Janiak, *Aust. J. Chem*, 2006, **59**, 22–25.